NMR IN BIOMEDICINE
NMR Biomed. 2007; **20**: 360–365
Published online in Wiley InterScience
(www.interscience.wiley.com) DOI:10.1002/nbm.1164

4D cardiac MRI in the mouse

Akiva Feintuch,[1]* Yonghong Zhu,[2] Jonathan Bishop,[1] Lorinda Davidson,[1] Jun Dazai,[1] Benoit G. Bruneau[2,3] and R. Mark Henkelman[1,4]

[1]Mouse Imaging Centre, Hospital for Sick Children, Toronto, Ontario, Canada
[2]Program in Cardiovascular Research, Hospital for Sick Children, Toronto, Ontario, Canada
[3]Department of Molecular and Medical Genetics, University of Toronto, Toronto, Ontario, Canada
[4]Department of Medical Biophysics and Radiology, University of Toronto, Toronto, Ontario, Canada

Received 5 November 2006; Revised 22 January 2007; Accepted 22 January 2007

ABSTRACT: With the introduction of mouse models for the study of cardiac morphogenesis, there arises a need for new imaging protocols that can capture both morphological and functional information. High-resolution 2D cardiac cine MRI has often been used to quantify left and right ventricular function. In this study we propose a 3D isotropic cardiac cine MRI protocol with a voxel size of 200 μm^3 as a means of studying cardiac multi-chamber morphology and function. A black blood sequence was used to enhance blood myocardium contrast. Manual segmentation of the ventricles was used to measure ventricular volumes at end diastole and end systole. This method is demonstrated on an *Irx4*-deficient mouse model. We have been able to identify the volumes of both ventricles dynamically and to show differences in ejection fraction in the mutant. We have also identified an abnormality of the papillary muscle in the mutant that had been missed in previous phenotyping with ultrasound and histology.

KEYWORDS: cardiac MRI; mouse; phenotyping

INTRODUCTION

Cardiac development is a multi-step process with different genes contributing at different stages of embryogenesis and at different locations within the developing heart (1,2). A better understanding of cardiac morphogenesis will contribute significantly to identifying the causes of congenital heart disease. To that end, numerous mouse models are being developed in which specific genes involved in cardiac development are modified. These mutations can result in defects in any of the four heart chambers, valves, septa, and great vessels and even in organs other than the heart. Assessment of these models requires imaging protocols that include structural and functional evaluation of all aspects of the heart including all four chambers.

Clinical ultrasound systems performing 3D/4D cardiac imaging with a linear array probe at 15 MHz have been previously tried for mouse cardiac phenotyping (3,4). In those studies the imaging is usually limited to the left ventricle probably because of the limited spatial resolution. High-frequency (20–50 MHz) ultrasound systems have been recently introduced for small-animal imaging (5) and have high spatial resolution [115 mm (lateral) × 55 mm (axial) at 30 MHz]. The real-time 2D imaging frame rate is up to 240 frames per second. However, only single-element mechanical transducers are available for these systems. Consequently, the data acquisition for 3D/4D cardiac imaging would be very time-consuming, and variations in heart rate and function will be introduced. Therefore evaluation of ventricular volume using high-frequency ultrasound is mainly based on two-dimensional imaging and the assumed 3D geometric shape of the observed structure.

High-resolution cine 2D mouse cardiac MRI has been previously demonstrated as a tool for quantifying mouse cardiac function (6–9). As is common in human cardiac MRI, a stack of 2D slices along the heart's main axis, with a slice thickness of 0.5–1 mm, is typically used for full heart coverage. Segmentation of ventricular volumes at end diastole and end systole are subsequently used to evaluate function. This method has been used successfully for evaluation of mouse models of myocardial infarct (6–8). Although 2D multi-slice imaging protocols are most common in human clinical imaging, significant effort has also been dedicated to 3D protocols, in some cases with isotropic voxels. The employment of 3D acquisition has long been considered mutually incompatible with the use of breath respiratory compensation, but with the continued evolution of free-breathing techniques, 3D isotropic cardiac imaging has become much more interesting to researchers (10,11). It appears to be especially attractive for coronary MR angiography

**Correspondence to:* A. Feintuch, MRI Unit, Soroka Medical Centre, P.O. Box 151, Beer Sheba, Israel, 84101.
E-mail: feintuch@phenogenomics.ca

Abbreviations used: *Irx*, Iroquois homeobox; MOTSA, multiple overlapping thin slabs; SNR, signal-to-noise ratio.

(12–14) because of the tortuous courses of the arteries. In mouse imaging, isotropic 3D post-mortem MRI has been used to measure the volumes of all four chambers in normal and cardiomyopathic mice (15), and was shown to agree with histology. The authors specifically noted the need to carry the technique forward to *in vivo* imaging. The implementation of *in vivo* isotropic cardiac mouse imaging can be significant for cardiac phenotyping where the location of the mutation is unknown. For an uncharacterized mouse cardiac mutant, *in vivo* isotropic imaging can potentially resolve structure and function of both ventricles as well as atrial anatomy, valvular function, and great vessel structure. Ruff *et al*. (16) have previously demonstrated *in vivo* cardiac 3D imaging for visualization of normal mouse coronary arteries and valves *in vivo*. In this paper we show 3D cine cardiac MRI with isotropic resolution and demonstrate its use in a mouse cardiac phenotyping application. We demonstrate that this method can provide a good perspective on morphology of all chambers as well as a good functional evaluation of the less uniform structures (right ventricle and possibly atria). The isotropic nature of the data enables viewing with equivalent image quality of retrospectively selected planes in arbitrary orientations. In addition, for a multi-subject study, as is typically required in phenotyping studies, 3D isotropic imaging is more general and less dependent on operator positioning of slices. Isotropic imaging can also be applied to multiple-mouse MRI to provide higher throughput (17).

The shorter cardiac cycle in mice relative to humans, and similar blood flow velocities (18), results in higher accelerations in the mouse and, as a result, losses in the blood MR signal. These in turn, as well as inflow effects, lead to diminished blood tissue contrast at certain stages of the cardiac cycle. 2D black blood mouse cardiac imaging was recently introduced (19) as a way to improve blood tissue contrast in mouse cardiac MR. We have adapted this method to 3D isotropic full heart imaging using a multiple overlapping thin slabs (MOTSA) technique (20).

The Iroquois homeobox (*Irx*) gene family comprises six genes encoding homeodomain-type transcription factors. All six *Irx* genes are expressed in different subdomains in the heart. Deletion of individual *Irx* genes results in mild or undetectable physiological phenotypes (21,22) including late-onset cardiomyopathy in *Irx4* knockout mice (23). In the case of *Irx4* knockout mice, no remarkable anomalies in cardiac structure were observed using ultrasound, but M-mode echocardiography detected decreased contractility and cardiac dilatation at 6 months of age (23).

METHODS

All animal utilization protocols were approved by the Hospital for Sick Children Animal Care Committee, subject to the Canadian Council on Animal Care.

The mice were anesthetized following induction with 4.0% isofluorane gas, and maintained with 1.6% gas with oxygen flowing at 1.2 L/min for a period of 3–4 h. The mice were loaded on positioning sleds (24) (Dazai Research Instruments, Toronto, Ontario, Canada), which included electrocardiograph electrodes fastened to the shaved chest with conductive hydro-gel, a pneumatic pillow for recording respiration, and cutaneous temperature monitoring. An SA Instruments Inc. (Edison, NJ, USA) system was used for cardiac monitoring and gating. The mice were breathing freely throughout all the scans and no respiratory gating was used. All imaging was performed on a Varian INOVA spectrometer using a 7 T, 40 cm horizontal bore magnet (Magnex Scientific Ltd, Oxford, UK). An insert gradient (Magnex Ltd.) with an inner diameter of 6 cm was used for shimming and spatial encoding. The maximal gradient used was 30 G/cm. A Millipede radio frequency coil with an inner diameter of 35 mm (Varian Inc., Palo Alto, CA, USA) was used for transmission and signal acquisition.

A low-flip-angle spoiled-gradient echo was used for prospectively gated cine imaging. Twelve phases were acquired for each cardiac cycle with a *TR* of 10–12 ms depending on the RR period (typically 120–180 ms for anesthetized mice) and a *TE* of 1.9 ms. The minimal *TR* permitted by the hardware was 9.5 ms. For bright blood imaging, a 3D acquisition of a 12 mm coronal slab centered on the heart was implemented. Imaging field of view was 48 mm × 24 mm × 12 mm with a matrix size of 240 × 120 × 60, resulting in isotropic voxels of 200 μm. The time for a single scan was 15–20 min (dependent on the heart rate), and the scan was repeated and averaged 4–6 times to obtain reasonable signal-to-noise ratio (SNR).

Black blood imaging was performed using a double inversion recovery sequence as described by Berr *et al*. (19). In this method, after a cardiac trigger, a non-selective 180° adiabatic pulse followed by a slab-selective 180° adiabatic pulse for re-inversion is performed. A line in k-space is acquired after the next cardiac trigger with 12 temporal phases (for a detailed diagram, see Berr *et al*. (19)). A MOTSA technique (20) with five overlapping coronal slabs was used to obtain full heart coverage. The thickness of each re-inverted slab was 3 mm followed by excitation of a 2.4 mm slab with 12 phase-encoding steps in the slab direction. For a coronal slab positioned at the center of the heart, a 3 mm slab can comprise up to half of the total cardiac blood volume. Thicker slabs resulted in non-satisfactory nulling of the blood signal. An overlap of 1.2 mm existed between adjacent slabs. Thus, the total thickness of the combined slabs was 7.2 mm (when the external edges were included), which gave total coverage of the heart blood volume, although anterior and posterior edges of the myocardium were at times left out. Spatial and temporal resolution were the same as with the bright blood. The time for a single scan was 40–50 min. It should be noted

DOI: 10.1002/nbm

that a single scan in this method is more than twice as long as in the bright blood method because of the double cardiac cycle period necessary for the inversion and the overlap of the slabs. The scan was repeated 3–4 times for averaging. Image reconstruction was performed in MATLAB. After reconstruction of each individual slab, the slabs were stitched together on the basis of slab position. Overlapping slices in different slabs were averaged to enhance SNR. A MATLAB histogram-equalization function was used to obtain a uniform intensity across the heart.

A group of three control (SvJ × BlackSwiss) and three *Irx4*$^{-/-}$ mice (25) aged 8–12 weeks were scanned with black blood contrast. Right and left ventricle segmentations at end systole and end diastole were performed manually by a single operator using 3D visualization software (AMIRA; Mercury Computer Systems, Chelmsford, MA, USA). An advantage of 3D isotropic data is that the segmentation can be carried out using all three views giving a consistent shape from any viewed direction. A smoothed (with a smoothing kernel 4 voxels wide) triangulated surface was then constructed in AMIRA from the 3D segmentation masks. The segmented volumes were then quantified and used for evaluation of cardiac function. An unpaired Student's *t*-test with equal variance was used to check for significant differences between the control and the mutant. An *F*-test was used to test for equal variance.

RESULTS

Short and long axis slices of a single wild-type mouse at end diastole and end systole, with both bright blood and black blood contrast, are shown in Fig. 1. All slices were reconstructed from a 3D acquisition and were obtained by an oblique slicing of the 3D image data along the long and short cardiac axes. The bright blood and black blood acquisitions were performed separately a few days apart. The bright blood images are clearly superior in SNR as expected, with an SNR of 18 for the myocardial signal in the bright blood sequence compared with a myocardial SNR of 10 for the black blood. The blood–myocardium border is clearer in the black blood images and improves segmentation results as previously shown by Berr *et al*. (19). For the purposes of this study, black blood contrast was used for improved segmentations.

Short axis slices at end diastole of the three *Irx4*$^{-/-}$ mice and three controls are shown in the upper row of Fig. 2. An enlarged and misplaced papillary muscle is

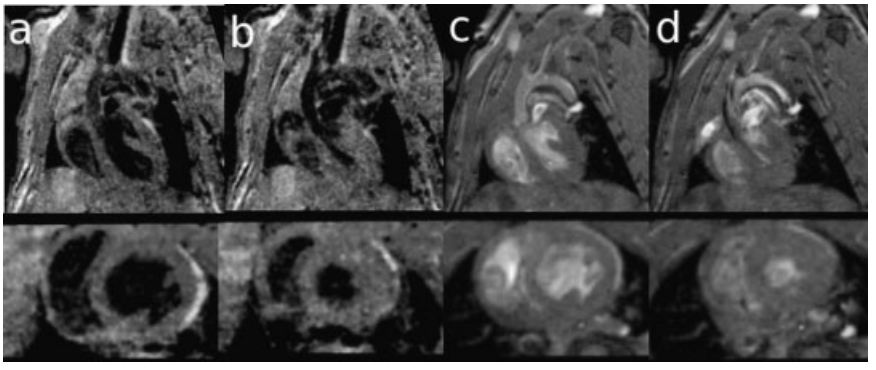

Figure 1. Long axis (top) and short axis (bottom) slices at end diastole (a,c) and end systole (b,d) with black blood (a,b) and bright blood (c,d) contrast. All slices were obtained by a retrospectively selected oblique cut through a 3D isotropic dataset. Time points represent two frames from a 12-phase movie loop. Data are from a 10-week-old control mouse (SvJ × BlackSwiss).

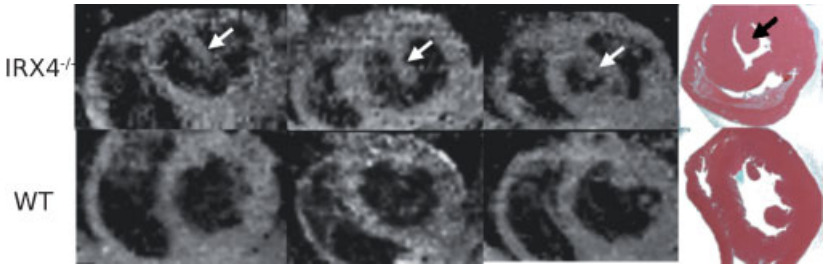

Figure 2. MRI from all six mice and histology (one from each) of *Irx4*$^{-/-}$ (IRX4; top) and wild-type (WT; bottom) showing the abnormality in the left papillary muscle of the mutant (*Irx4*$^{-/-}$) mice (arrows).

DOI: 10.1002/nbm

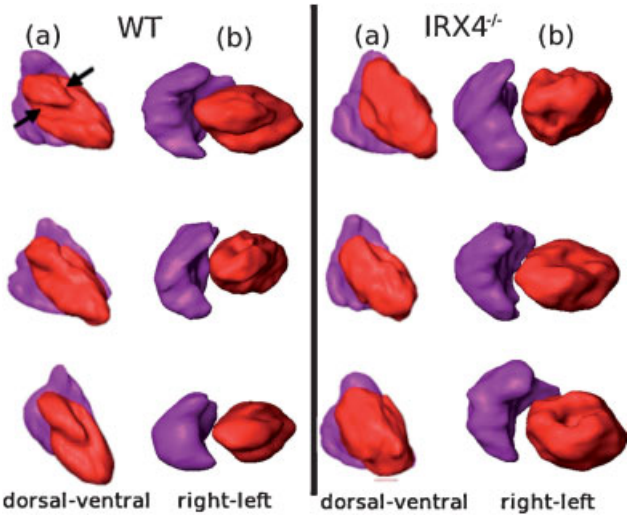

Figure 3. Isosurface renderings of the segmented volumes of the right (purple) and left (red) ventricles at end diastole as viewed from two different angles (a+b). The left column shows the three control mice (WT) and the right the three *Irx4*$^{-/-}$ (IRX4$^{-/-}$) mice. The normal positioning of the papillary muscle is indicated by arrows on the top left view.

clearly seen on all three *Irx4*$^{-/-}$ mice. The same effect is seen on histological slices shown in the bottom half of Fig. 2. This anomalous papillary muscle has not been identified in previous studies, but on retrospect can be seen as a faint additional intermediate echo on M-mode ultrasound [25].

Surface renderings of the segmented right and left ventricles at end diastole of three wild-type mice and three *Irx4*$^{-/-}$ mice are shown in Fig. 3 from two different viewing angles. A difference in left ventricular morphology is clearly noticeable in the *Irx4*$^{-/-}$ mice. In view angle (a), the outflow tract is pointed upwards and the dilation of the left ventricle in the *Irx4*$^{-/-}$ mice is apparent. In view angle (b), the outflow tract is pointing out of the page, and in the *Irx4*$^{-/-}$ mice voids in the blood volume can be seen caused by the anomaly in the papillary muscle. No morphological differences were visible in the right ventricle. The quantitative measurements summarized in Table 1 show the left ventricle of the *Irx4*$^{-/-}$ mice to be dilated. Both left ventricle end-diastolic volume and end-systolic volume were larger in the mutant mice. Ejection fractions of the *Irx4* mutant mice were typically lower, although the difference did not reach statistical significance ($P = 0.11$). This is consistent with previous ultrasound measurements [25] performed at a later age. In those measurements, the left ventricular end-diastolic and end-systolic diameter were measured at 24 weeks for the *Irx4*$^{-/-}$ mutant (mean $\pm$ SD 3.65 ± 0.15 mm and 2.22 ± 0.22 mm respectively) and the wild-type (3.37 ± 0.17 mm and 1.51 ± 0.20 mm respectively) showing an enlarged left ventricle in the mutant. The fractional shortening was significantly larger in the mutant ($40\% \pm 4\%$) than the wild-type ($55\% \pm 2\%$). The right ventricle of the mutant, measured here for the first time, exhibits normal size and function, consistent with the qualitative morphological assessment.

DISCUSSION

The development of mouse models of human disease over the past few years has necessitated the adaptation of human imaging methods to mice. Such has been the case in mouse cardiac MRI. Acquisition of 2D slices perpendicular to the long axis of the heart typically used in humans to evaluate left ventricular function has been directly transferred to the mouse. In this paper, we show that, because of differences in both the purpose of the scans and the imaging environment, 3D isotropic imaging plus time (known as 4D imaging) should be considered as an alternative and is feasible for mouse cardiac phenotyping applications.

Table 1. Quantitative measurements of the left and right ventricles of three control mice (WT) and three *Irx4*$^{-/-}$ (IRX4) mice. LVEDV, Left ventricular end-diastolic volume; LVESV, left ventricular end-systolic volume; LVSV, left ventricular stroke volume; LVEF, left ventricular ejection fraction; RVEDV, right ventricular end-diastolic volume; RVESV, right ventricular end-systolic volume; RVSV, right ventricular stroke volume; RVEF, right ventricular ejection fraction

	LVEDV (μL)	LVESV (μL)	LVSV (μL)	LVEF (%)	RVED (μL)	RVES (μL)	RVSV (μL)	RVEF (%)
WT_1	47	13	33	71	44	14	30	67
WT_2	44	11	33	75	41	10	31	75
WT_3	42	14	28	66	45	21	24	54
Mean ± SD	44 ± 3	13 ± 2	31 ± 3	71 ± 5	43 ± 2	15 ± 5	28 ± 4	65 ± 11
IRX4_1	49	17	32	66	41	12	29	71
IRX4_2	63	24	39	61	52	17	35	67
IRX4_3	60	32	28	46	41	12	29	71
Mean ± SD	57 ± 7* ($p = 0.04$)	24 ± 8 ($p = 0.05$)	33 ± 6	58 ± 10 ($p = 0.11$)	44 ± 6	13 ± 3	31 ± 4	69 ± 2

Function of both ventricles quantified by manual segmentation. L(R)VED – left(right) ventricle volume end diastole, L(R)VES – left (right) ventricle volume end systole, L(R)VSV – left(right) ventricle stroke volume, L(R)VEF – left(right) ventricle ejection fraction.

DOI: 10.1002/nbm

When human and mouse imaging are compared, a number of factors are germane. A major obstacle in human cardiac MRI is severe ghosting caused by respiratory motion. In the data presented in this paper, although respiratory gating was not used, respiratory ghosting is not apparent (Fig. 1) and seems to be averaged out as a result of the additional phase-encoding dimension, as has been previously reported (16,26). Thus, none of the ultra-fast breath-hold techniques developed for humans are required. In addition, the shorter cardiac cycle enables faster repetition times, shortening total scan time. The total scan time feasible in anesthetized mice is 3–4 h, whereas in an average human it is limited to 1 h. Consequently the additional averaging in mice enables reasonable SNR at an appropriate isotropic resolution. Nevertheless, improved SNR, possibly using phased-array coils, would be highly advantageous in mice as it has been proved to be in cardiac imaging of humans (27).

The *Irx4* knockout mouse used in this work has been previously phenotyped using echocardiography at 6 weeks and at 24–30 weeks, showing impaired left ventricular function in the latter adult group, manifest as increased end-systolic and end-diastolic dimensions. This trend was confirmed in this study, although statistical significance for the lower ejection fraction was not reached, indicating in the younger mice analyzed here a defect that was previously detected only in older mice by echocardiography. Right ventricular function was not measured by ultrasound, as an appropriate window for right ventricle viewing is lacking in the mouse. Right ventricle anatomy and function were measured here for the first time using MR and shown in this mutation to be normal. In addition, we have shown an abnormality of the papillary muscle, which has not been previously observed. The three-dimensionality of the data enabling arbitrary retrospective oblique slicing was beneficial for the observation of this new phenotype.

For this study, black blood contrast was chosen using a double inversion preparation and a MOTSA technique. Although reasonable results were achieved enabling manual segmentation of the ventricles, this acquisition strategy is less than ideal. As shown in Fig. 1, this method results in lower SNR compared with a standard spoiled 3D gradient echo. In addition, the loss of blood signal is both slab and time dependent resulting in moderate artifacts in the stitched images. For future work, other alternatives should be considered. Possible options are optimization of the bright blood signal to overcome motion de-phasing (by shorter echo times) or blood blanking contrast agents such as iron particulates. Improved contrast for blood in either direction will serve to enhance the advantage already shown to be inherent in 3D isotropic imaging of the heart. Contrast improvements will also facilitate automatic computer segmentation of the chambers, a requirement for serious phenotyping.

As a final note, when the 'big picture' of mouse imaging for phenotyping is considered, the need for high throughput has to be taken into account (17). An initial attempt at multiple-mouse cardiac imaging has been recently reported (26). For such an implementation, where all mice share a common gradient field, the positioning of a shared orientation capturing short and long axis views of the hearts of all mice will be an extremely difficult task. A working 3D isotropic cardiac imaging protocol is another important step towards the use of multiple-mouse live cardiac imaging.

Acknowledgements

We thank Dr S. Berr and Dr F. Epstein (University of Virginia) for providing the black blood contrast sequence. This work is part of the Mouse Imaging Centre (MICe) at the Hospital for Sick Children and the University of Toronto. The infrastructure has been funded by the Canada Foundation for Innovation (CFI) and Ontario Innovation Trust (OIT). The research has been funded by an Ontario Research and Development Challenge Fund (ORDCF) grant to the Ontario Consortium for Small Animal Imaging (OCSAI). Work on *Irx* genes in the laboratory of B.G.B. is funded by the Canadian Institutes of Health Research (CIHR).

REFERENCES

1. Bruneau BG. The developing heart and congenital heart defects: a make or break situation. *Clin Genet.* 2003; **63**(4): 252–261.
2. Gruber PJ, Epstein JA. Development gone awry: congenital heart disease. *Circ Res.* 2004; **94**(3): 273–283.
3. Dawson D, Lygate CA, Saunders J, Schneider JE, Ye X, Hulbert K, Noble JA, Neubauer S. Quantitative 3-dimensional echocardiography for accurate and rapid cardiac phenotype characterization in mice. *Circulation.* 2004; **110**(12): 1632–1637.
4. French BA, Li Y, Klibanov AL, Yang Z, Hossack JA. 3D perfusion mapping in post-infarct mice using myocardial contrast echocardiography. *Ultrasound Med. Biol.* 2006; **32**(6): 805–815.
5. Foster FS, Pavlin CJ, Harasiewicz KA, Christopher DA, Turnbull DH. Advances in ultrasound biomicroscopy. *Ultrasound Med. Biol.* 2000; **26**(1): 1–27.
6. Ruff J, Wiesmann F, Hiller KH, Voll s, Von Kienlin M, Bauer WR, Rommel E, Neubauer S, Haase A. Magnetic resonance microimaging for noninvasive quantification of myocardial function and mass in the mouse. *Magn Reson Med.* 1998; **40**: 43–48.
7. Slawson SE, Roman BB, Williams DS, Koretzky AP. Cardiac MRI of the normal and hypertrophied mouse heart. *Magn Reson Med* 1998; **39**: 980–987.
8. Wiesmann F, Frydrychowicz A, Rautenberg J, Illinger R, Rommel E, Haase A, Neubauer S. Analysis of right ventricular function in healthy mice and a murine model of heart failure by *in vivo* MRI. *Am J Physiol Heart Circ Physiol* 2002; **283**: 1065–1071.
9. Wiesmann F, Ruff J, Engelhardt S, Hein L, Dienesch C, Leupold A, Illinger R, Frydrychowicz A, Hiller K, Rommel E, Haase A, Lohse MJ, Neubauer S. Dobutamine-stress magnetic resonance microimaging in mice. *Circ. Res.* 2001; **88**(6): 563–569.
10. Fenchel M, Greil GF, Martirosian P, Kramer U, Schick F, Claussen CD, Sieverding L, Miller S. Three-dimensional morphological magnetic resonance imaging in infants and children with congenital heart disease. *Pediatr Radiol.* 2006; Sep 28; [Epub ahead of print]

DOI: 10.1002/nbm

11. Sorensen TS, Beerbaum P, Korperich H, Pedersen EM. Three-dimensional, isotropic MRI: a unified approach to quantification and visualization in congenital heart disease. *Int J Cardiovasc Imaging.* 2005; **21**: 283–292.
12. Botnar RM, Stuber M, Kissinger KV, Manning WJ. Free-breathing 3D coronary MRA: the impact of ''isotropic'' image resolution. *J Magn Reson Imaging.* 2000; **11**: 389–393.
13. Stehning C, Bornert P, Nehrke K, Eggers H, Dossel O. Fast isotropic volumetric coronary MR angiography using free-breathing 3D radial balanced FFE acquisition. *Magn Reson Med.* 2004; **52**: 197–203.
14. Weber OM, Martin AJ, Higgins CB. Whole-heart steady-state free precession coronary artery magnetic resonance angiography. *Magn Reson Med.* 2003; **50**: 1223–1228.
15. Sze RW, Chan CB, Dardzinski BJ, Dunn S, Sanbe A, Schmithorst V, Robbins J, Holland SK, Strife JL. Three-dimensional MR microscopy of a transgenic mouse model of dilated cardiomyopathy. *Pediatr Radiol.* 2001; **31**: 55–61.
16. Ruff J, Wiesmann F, Lanz T, Haase A. Magnetic resonance imaging of coronary arteries and heart valves in a living mouse: techniques and preliminary results. *J Magn Reson* 2000; **146:** 290–296.
17. Bock NA, Konyer NB, Henkelman RM. Multiple-mouse MRI. *Magn Reson Med* 2003; **49**: 158–167.
18. Janssen B, Debets J, Leenders P, Smits J. Chronic measurement of cardiac output in conscious mice. *Am J Physiol Regul Integr Comp Physiol* 2002; **282**(3): R928–R935.
19. Berr SS, Roy RJ, French BA, Yang Z, Gilson W, Kramer CM, Epstein FH. Black blood gradient echo cine magnetic resonance imaging of the mouse heart. *Magn Reson Med* 2005; **53**: 1074–1079.
20. Parker DL, Yuan C, Blatter DD. MR angiography by multiple thin slab 3-D acquisition. *Magn. Reson. Med.* 1991; **17**: 434–451.
21. Lebel M, Agarwal P, Cheng CW, Kabir MG, Chan TY, Thanabalasingham V, Zhang X, Cohen DR, Husain M, Cheng SH, Bruneau BG, Hui CC. The Iroquois homeobox gene Irx2 is not essential for normal development of the heart and midbrain-hindbrain boundary in mice. *Mol Cell Biol.* 2003; **23**(22): 8216–8225.
22. Costantini DL, Arruda EP, Agarwal P, Kim KH, Zhu Y, Zhu W, Lebel M, Cheng CW, Park CY, Pierce SA, Guerchicoff A, Pollevick GD, Chan TY, Kabir MG, Cheng SH, Husain M, Antzelevitch C, Srivastava D, Gross GJ, Hui CC, Backx PH, Bruneau BG. The homeodomain transcription factor Irx5 establishes the mouse cardiac ventricular repolarization gradient. *Cell.* 2005; **123**(2): 347–358.
23. Bruneau BG, Bao ZZ, Fatkin D, Xavier-Neto J, Georgakopoulos D, Maguire CT, Berul CI, Kass DA, Kuroski-de Bold ML, de Bold AJ, Conner DA, Rosenthal N, Cepko CL, Seidman CE, Seidman JG. Cardiomyopathy in Irx4-deficient mice is preceded by abnormal ventricular gene expression. *Mol Cell Biol.* 2001; **21**(5): 1730–1736.
24. Dazai J, Bock NA, Nieman BJ, Davidson LM, Henkelman RM, Chen XJ. Multiple mouse biological loading and monitoring system for MRI. *Magn Reson Med* 2004; **52**: 709–715.
25. Bruneau BG, Bao Z-Z, Fatkin D, Xavier-Neto J, Georgakopoulos D, Maguire CT, Berul CI, Kass DA, Kuroski-de Bold ML, de Bold AJ, Conner DA, Rosenthal N, Cepko CL, Seidman JG, Seidman CE. Cardiomyopathy in Irx4-deficient mice is preceded by aberrant ventricular gene expression. *Molecular and Cellular Biology* 2001; **21**(5): 1730–1736.
26. Bishop J, Feintuch A, Bock AN, Nieman B, Dazai J, Davidson L, Henkelman RM. Retrospective gating for mouse cardiac MRI. *Magn Reson Med* 2006; **55**(3): 472–477.
27. Wintersperger BJ, Reeder SB, Nikolaou K, Dietrich O, Huber A, Greiser A, Lanz T, Reiser MF, Schoenberg SO. Cardiac CINE MR imaging with a 32-channel cardiac coil and parallel imaging: impact of acceleration factors on image quality and volumetric accuracy. *J Magn Reson Imaging.* 2006; **23**(2): 222–227.

DOI: 10.1002/nbm